JACS
JOURNAL OF THE AMERICAN CHEMICAL SOCIETY
Article
pubs.acs.org/JACS

Kinetics and Thermodynamics of Watson–Crick Base Pairing Driven DNA Origami Dimerization

John Zenk,[†] Chanon Tuntivate,[†] and Rebecca Schulman*[,†,‡]

[†]Chemical and Biomolecular Engineering and [‡]Computer Science, Johns Hopkins University, Baltimore, Maryland 21218, United States

Supporting Information

ABSTRACT: We investigate the kinetics and thermodynamics of DNA origami dimerization using flat rectangle origami components and different architectures of Watson–Crick complementary single-stranded DNA ("sticky end") linking strategies. We systematically vary the number of linkers, the length of the sticky ends on the linker, and linker architecture and measure the corresponding yields as well as forward and reverse reaction rate constants through fluorescence quenching assays. Yields were further verified using atomic force microscopy. We calculate values of $H°$ and $\Delta S°$ for various interface designs and find nonlinear van't Hoff behavior, best described by two linear equations, suggesting distinct regimes of dimerization between those with and those without well-formed interfaces. We find that self-assembly reactions can be tuned by manipulating the interface architecture without suffering a loss in yield, even when yield is high, ∼75–80%. We show that the second-order forward reaction rate constant (k_{on}) depends on both linker architecture and number of linkers used, with typical values on the order of 10^5–10^6 $(M·s)^{-1}$, values that are similar to those of bimolecular association of small, complementary DNA strands. The k_{on} values are generally non-Arrhenius, tending to increase with decreasing temperature. Finally, we use kinetic and thermodynamic information about the optimal linking architecture to extend the system to an infinite, two-component repeating lattice system and show that we can form micron-sized lattices, with well-formed structures up to 8 μm^2.

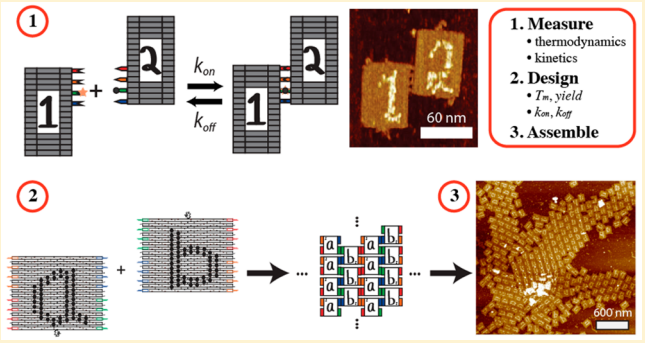

INTRODUCTION

With the advent of DNA origami[1] came the possibility of high-resolution nanobreadboards, enabling unprecedented control of matter on the nanoscale.[2] This feature has allowed the creation of DNA origami nanodevices that promise many potentially useful applications, including nanoscale reactors[3] and devices,[4] molecular robots,[5] sensors and actuators,[6] devices to control self-assembly,[7] novel drug delivery systems,[8] and molecular tools to probe or mimic biological components.[9]

One major limitation of these technologies is the amount of surface area of an individual origami onto which molecular components can be placed with nanoscale resolution, which is typically limited by the size of the DNA scaffold (usually ∼7 kb). Therefore, the surface area of the origami only affords attachment of a small number of components, limiting the complexity and utility of the devices.[10] Many methods have been proposed to overcome this problem: origami have been made from multiple scaffolds,[11] individual origami have been assembled or organized into complexes,[12] and surfaces have been used to confine the geometry in order to enhance self-assembly outcomes.[13] The thermodynamics and kinetics of smaller DNA tiles have been well-studied.[14] Two- and three-dimensional DNA origami have been extensively characterized, computationally modeled, and built with various interorigami geometries.[15] However, a systematic characterization of interfaces involving DNA origami components has yet to be accomplished.

Recent successes in the design of protein assemblies, including the successful design and assembly of protein-only 2D infinite lattices[16] and finite complexes,[17] suggest that predicting structure and tuning interfacial energies using data-driven computational modeling software[18] is essential to optimize self-assembly outcomes. If DNA nanotechnologists are to reliably build larger, more complex architectures using a DNA origami breadboard, an understanding of origami interfaces, including kinetics and thermodynamics, is required.[2]

Our goal in this paper is to understand how to control the strength and reversibility of interfacial reactions between origami components when assembly is driven by the Watson–Crick (WC) hybridization of multiple sets of short "sticky ends" (SEs). We chose this architecture because large libraries of such interfaces with low cross-talk can be designed,[19] suggesting a way to rapidly scale the complexity of assembly reactions. We characterized the dimerization of origami tiles using a fluorescence-quenching assay and

Received: October 19, 2015
Published: February 29, 2016

DOI: 10.1021/jacs.5b10502
J. Am. Chem. Soc. 2016, 138, 3346–3354

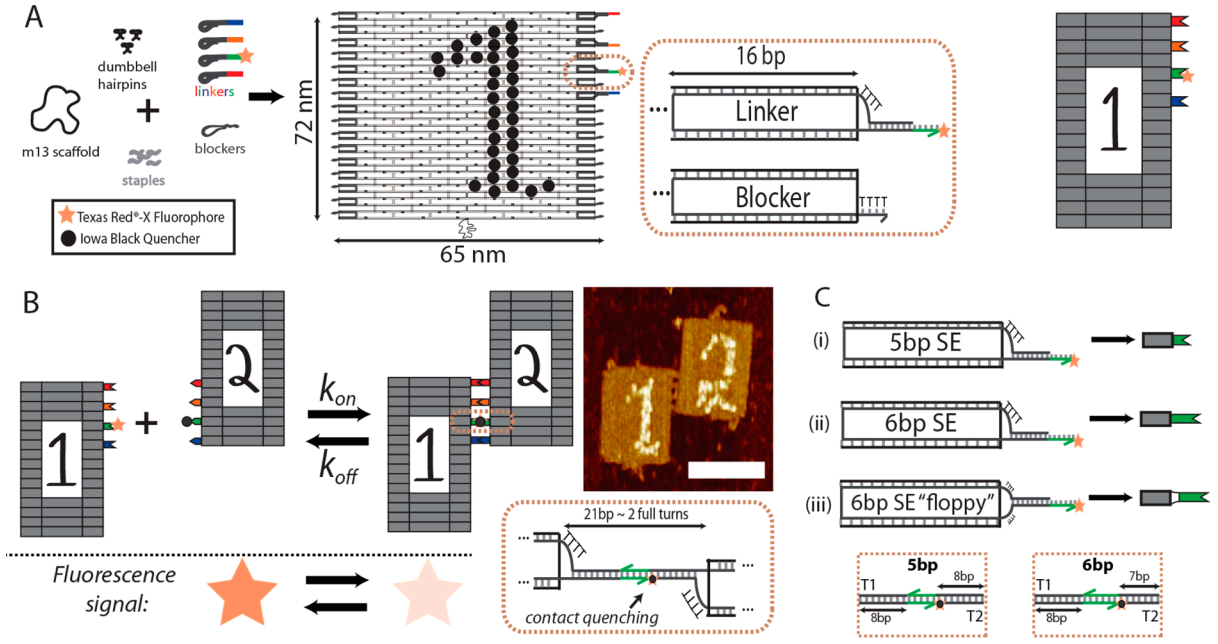

Figure 1. Schematic of the DNA origami tile dimer system. (A) DNA origami monomers (T1 shown) are assembled by annealing the scaffold with hairpins, blockers, linkers, and staples. Hairpins label tiles by providing height contrast on an AFM image. Blockers mitigate nonspecific interactions between origami, such as blunt-end stacking. Linkers facilitate interaction specificity through a single-stranded "sticky end" (SE) domain. (Far right) Schematic of T1 and its interface. (B) Dimer formation occurs via SE hybridization. Complementary linkers in diagrams have the same color and complementary shapes. A fluorophore−quencher pair, drawn as an orange star and black circle, respectively, which is attached to the SE (colored green), is used to track the dimerization process. AFM image shows the assembled dimer. Scale bar is 60 nm. (C) The different linker architectures investigated in this work, including linkers with (i) 5 bp (base pair) SEs, (ii) 6 bp SEs, (iii) 6 bp floppy SEs (two polythymine regions after the scaffold-complementary region). Inset diagrams show linking architecture between T1 (left) and T2 (right) for 5 and 6 bp linkers. For all interfaces, a 5′ Iowa Black RQ on T2 quenches a 3′ Texas Red-X NHS Ester on T1.

correlated this assay to a robust but low-throughput measure of dimer yield, visual characterizations using an atomic force microscope (AFM). We measured multiple thermodynamic and kinetic parameters, including yield, melting temperature, reaction rate constants, and $\Delta H°$ and $\Delta S°$ using the van't Hoff equation. We tested multiple different interface design strategies, including modifying the number of linkers per interface, their positional arrangement on the interface, SE length, and linker flexibility. We found that (1) yield generally increases or remains constant with the number of linkers; (2) reaction outcomes can be tuned via interface design in order to change the dimer melting temperature while maintaining high yields; (3) dimerization occurs rapidly, with forward reaction rate constants comparable to smaller, DNA tile dimerization and complementary oligonucleotide hybridization reactions, which could suggest a unified design strategy for hierarchical DNA assembly processes; and (4) we can use the information obtained about component interfaces in the dimerization assays to inform the design of a self-assembly system for 2D infinite lattices.

RESULTS AND DISCUSSION

As an example component for hierarchical assembly reactions involving origami components, we considered the dimerization of two 2D DNA origami rectangle tiles. The components were designed with caDNAno[15c] to be planar, with a twist near to that of B-form DNA, i.e., 10.44 bases per turn, similar to a previously described origami structure.[20] CanDO[21] modeling software also predicted that the resulting origami structure would have little global twist (Supporting Information, Figure S1). Hairpin staples assembled in specific positions on the two separate components allow the first component (labeled with a series of hairpins to depict the number "1", called T1) to be distinguished from the second component (labeled with a series of hairpins to depict the number "2", called T2) in AFM images (Figure 1A). The hairpins may induce unpredictable curvature to the origami components.[22] As homogeneous interfaces appear to bind to one another more effectively than heterogeneous interfaces,[23] the system was designed such that the set of scaffold sequences in the interfacial domain on T1 and T2 are the same. Therefore, upon dimerization T2 is rotated 180° in plane relative to T1 in the dimer.

The interface for binding between the two components consisted of blocker edge staples, which help prevent nonspecific interactions such as blunt-end stacking, and linker edge staples, which facilitate specific interactions between components via WC base pairing. Blocker edge staples contain a single-stranded polythymine (Thy4) domain on the 3′-end, to mitigate blunt-end stacking.[24] Linker staples consist of five domains: a domain complementary to the origami scaffold, one or two Thy4 domains to allow linkers to traverse helices, two complementary intralinker domains, and a SE domain the sequence of which is complementary to the opposite component. The linkers were designed so that upon dimerization, the two origami components are separated by 21 bases, or approximately two full turns assuming B-form DNA,[25] so that the dimer would have an effectively planar structure (Figure 1B,C).

To understand how interface structure determines binding energy and the kinetics of component binding, we systematically altered three variables: (1) the number and (2) arrangement of the linkers at the interface and (3) the length

DOI: 10.1021/jacs.5b10502
J. Am. Chem. Soc. 2016, 138, 3346−3354

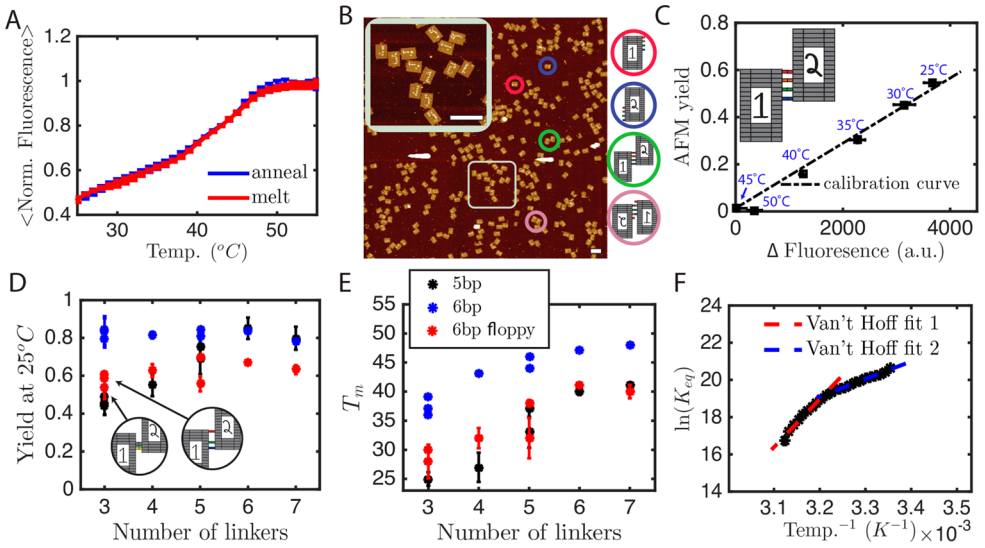

Figure 2. Measurement of dimerization yield and thermodynamic parameters. (A) Typical anneal/melt fluorescence curve depicting the averaged, normalized fluorescence of three mixtures of T1 and T2 with the same interface design that are cooled and then heated across a range of temperatures to produce a reversible binding transition (floppy four SE interface shown). (B) AFM scan of a T1−T2 mixture. Potential products include T1 alone (red), T2 alone (blue), the dimer D in correct orientation (green), and the dimer D in flipped confirmation (pink). Scale bars are 200 nm. (C) Normalized fluorescence measurements of dimerization yield are linearly related to measurements of yield determined from AFM micrographs and were used to quantitatively measure origami yield (5 bp four SE interface shown). All yield−fluorescence calibration measurements were made with the four-linker architecture (as seen in the inset diagram). (D) Dimer yield and (E) melting temperature (T_m, defined as the temperature at which the yield is 50%), as a function of linker architecture and number of linkers. Multiple data points at a given number of linkers indicate different linker arrangement on the origami, as seen in the inset of panels D and E; the color key is the same in both plots. (F) Equilibrium constants of dimer binding as a function of temperature, shown as a van't Hoff plot. The curve shape is typical of origami dimerization for the systems we studied, with two different linear regions. Error bars indicate one standard deviation of the reported quantity and are too small to be seen in panel F. Bootstrapping is used to determine error bars for the AFM yield and are too small to see in panel C.

of each SE. We considered the binding of components with interfaces containing between 3 and 7 linker pairs with either 5 or 6 base pair (bp) SEs. For interfaces with 3 and 5 linkers we tested multiple positional arrangements of the linkers.

We also tested the effects of linker flexibility by comparing linkers with and without a pair of Thy4 domains between the origami structure and the intralinker complementary region; we call such linkers with a pair of Thy4 domains "floppy" linkers (Figure 1C). SE sequences were designed to reduce cross-talk and have approximately the same interaction energy per SE[26] (Supporting Information, Note 6).

To quantitatively characterize yield and rates of dimerization, we used a fluorescence quenching assay where the 3′-end of one of the linking strands on T1 was modified with a Texas-Red-X (NHS Ester) fluorophore and the 5′-end of the complementary T2 linker was modified with Iowa Black RQ quencher so that dimerization produces a decrease in fluorescence[27] (Figure 1B). To ensure that the fluorophore−quencher interaction was solely responsible for changes in fluorescence upon binding, we performed control experiments where a fluorescently labeled T1 reacted with T2 with and without a quencher. We found that upon dimerization with a quencher, the reaction produced a dramatic decrease in fluorescence while dimerization without a quencher actually slightly enhanced fluorescence upon binding (Supporting Information, Figure S3). To investigate whether the quenching effect was a result of origami binding or simply the complementary linkers binding in solution, we performed another control experiment where we mixed solutions of the T1 and T2 staples and linkers only, which produced no fluorescence change for 5 bp linkers (Supporting Information, Figure S4). About 5% of floppy linkers dimerize or bind to an origami interface at 25 °C (Supporting Information, Figure S5A). Binding between free linkers with 6 bp SEs produced a significant fluorescence change below 35 °C (Supporting Information, Figure S5B) and indicated a ∼20% yield at 25 °C. The binding energy of origami dimerization for a given temperature can be measured by determining the yield of dimerization at equilibrium for known concentrations of monomer reactants. To find an assembly protocol that would stay close to equilibrium as the temperature was changed, we mixed 5 nM of each of the two origami monomer types at equal concentrations (see the methods) and measured the fluorescence at different temperatures for a set of different annealing and melting speeds. We found that for linkers with 5 bp SE and floppy linkers, there was no significant hysteresis between 25 and 55 °C when the temperature decreased at 1 °C per 15 min during annealing and increased at 1 °C per 15 min during melting (Figure 2A and Supporting Information, Figures S7, S8, S11, and S12), suggesting that the system stayed close to equilibrium during both the heating and cooling processes. Decreasing the melting and cooling rates did not significantly change fluorescence values at any point during the process (Supporting Information, Figure S13). The interfaces with four to seven 6 bp SE linkers required a longer time at each temperature to achieve equilibrium, as hysteresis was observed when melted and annealed using the above protocol. Thus, samples with these interfaces were heated and cooled at a rate of 1 °C per 60 min (Supporting Information, Figures S9, S10, and S14). In some cases the fluorescence signals from the first melt were noisy compared to the signal from subsequent anneal and melt cycles, which may be due to noise in the fluorescence signal (Supporting Information, Note 2). To collect fluorescence data, we therefore melted and annealed each pair of

DOI: 10.1021/jacs.5b10502
J. Am. Chem. Soc. 2016, 138, 3346−3354

components for at least 1.5 cycles (melt → anneal → melt) and excluded data from the first melt. In all anneal and melt experiments, the temperature never reached the melting temperature of the origami components (Supporting Information, Figure S2).

Fluorescence-Quenching Assay Can Be Used as a Proxy for Dimer Yield with Proper Calibration. To verify that the fluorescence signal from these experiments could be used to determine dimerization yield, we also measured the yield of origami dimers at different temperatures using atomic force microscopy. We scanned random portions of a mica puck prepared after an assembly reaction proceeded in solution at a particular temperature (see the methods), and using the labels on each component, we classified the observed assemblies as either T1, T2, D (dimer), or a flipped dimer (Figure 2B). By combining the AFM data with the fluorescence-quenching assay data, we correlated the change in fluorescence to dimer yield and produced a calibration curve that indicated that the two measurements were linearly related (Figure 2C). To account for differences in fluorescence-quenching efficiency for different linker architectures, we produced different calibration curves for each linker architecture using a distinct set of AFM measurements of yield (Supporting Information, Figure S6) and used these calibration curves to convert fluorescence signals into a quantitative measure of yield. Notably, yield did not approach 1 at the coldest temperature studied in these curves, but instead, yield varied widely at that temperature, depending on interface design. In producing the calibration curves, we assumed that quenching efficiency varies only with linker architecture (i.e., SE length and whether the linker contains a Thy4 insert) and not with the number of SEs, as the linker architecture is the determining factor for the positions of the quencher and fluorophore, which ultimately determine fluorescence-quenching efficiency.

Dimer Yield at 25 °C Tends To Increase with Number of Linkers Per Interface but Saturates at ∼80% Yield. We found that in most cases, yield is strongly dependent on temperature, as would be expected for a reaction driven by DNA hybridization.[28] However, unlike the hybridization of two DNA strands, the melting transition was very broad, with yields between the minimum and maximum stretching over more than 20 °C for most types of interfaces (Supporting Information, Figures S7−S12). We found that for 5bp and floppy linkers, increasing the number of linkers, up to about six per interface (Figure 2D), tended to increase yield. Increasing the number of linkers to more than six did not necessarily produce a higher yield. This result echoes studies performed on the energetics of interaction between smaller DNA nanostructures, where increasing the number of linkers above a threshold did not increase the melting temperature.[14b] However, linkers with 6 bp SEs produced higher yields than floppy linkers at all temperatures tested, with yields remaining high and approximately constant as the number of linkers per interface increased. The interface with three short 5 bp SEs produced the smallest yield of any interface, which is likely because the interactions between these sticky ends are not strong enough to maintain a bond between origami components. Interfaces with 6 bp linkers produced the highest yields up to about five linkers per interface; thereafter, the 5 and 6 bp linkers had similar yields. Furthermore, while the arrangement of the linkers is important, there was not a clear pattern as to how linker arrangements affect interface energetics; one possibility is that arrangements of linkers that could form with relatively little structural distortion produced stronger interactions.

In the AFM images, most of the SEs between dimers appeared to be bound, although this might not be the case in solution. One important result deduced from AFM imaging is that the maximum yield of dimers for the temperatures we studied is well below 100%. The maximum yield we obtain at 25 °C is ∼80% (Figure 2D). We hypothesized that this relatively low maximum yield could be caused by linker swapping, where linkers or edge staples with the same scaffold complementary could swap positions with a specific linker, reducing the strength of the interface. However, we found that less than ∼5% of linkers swap positions when heated to 55 °C, suggesting that linker swapping is not the major mechanism limiting binding yield (Supporting Information, Figure S30). We then hypothesized that yield limitations could be caused by the fact that linkers were purchased with standard desalting and were not purified, so that linkers that are defective or truncated due to synthesis errors could be incorporated into the origami, affecting the binding properties of the interface. To test this hypothesis, we obtained yield measurements via AFM for origami with PAGE-purified linkers in the 6 bp four SE interface. When directly comparing the yields measured with AFM at 25 °C, we see that the yield achieved with purified linkers was 83%, or about 10% higher than the case of linkers that are synthesized with standard desalting (Supporting Information, Figure S9). Although incremental improvements in yield can be achieved via linker purification, the modest yield enhancements might not be worth the typically high cost or laborious process of purification, especially if larger, more complex, multicomponent systems were to be created. It is not clear whether limitations on yield are due to imperfections in the structures being assembled (so that some structures never participate in a binding reaction) or whether origami interfaces reversibly achieve an equilibrium yield of significantly less than 1 over a broad range of temperatures. Importantly, these results suggest that studies of DNA nanostructure hybridization should not assume maximal yield at low temperatures but instead should calibrate fluorescence studies using a separate metric.

Melting Temperature Generally Increases with the Number of Linkers Per Interface. We next wanted to determine how the different interface designs affected the thermal stability of the dimer, so we calculated the melting temperature, T_m, defined as the temperature at which the yield is 50%. For all linkers, the T_m increased on average as the number of linkers in an interface increased (Figure 2E), suggesting that multivalent interactions provide thermal stability to the structure. This effect has been observed in the assembly of smaller DNA tiles[14b] and also in DNA-mediated colloid assembly,[29] where increasing the surface density of SEs per colloid increases the T_m. Floppy linkers produced lower T_m values than nonfloppy linkers for all of the number of linkers per interface studied and had similar T_m values to interfaces with 5 bp SEs. Floppy linkers have a larger entropic penalty for forming contacts due to the increased configurational space for linkers to explore, as the poly-T region adds additional translational and rotational degrees of freedom, which likely reduce the thermal stability of the dimer. In general, this method of adding more linkers to an interface can be used to thermally tune a self-assembly reaction. In fact, in the case of 6 bp linkers, one could modulate the number of linkers per interface, thereby tuning the thermal properties of the reaction, without suffering a loss in yield.

DOI: 10.1021/jacs.5b10502
J. Am. Chem. Soc. 2016, 138, 3346−3354

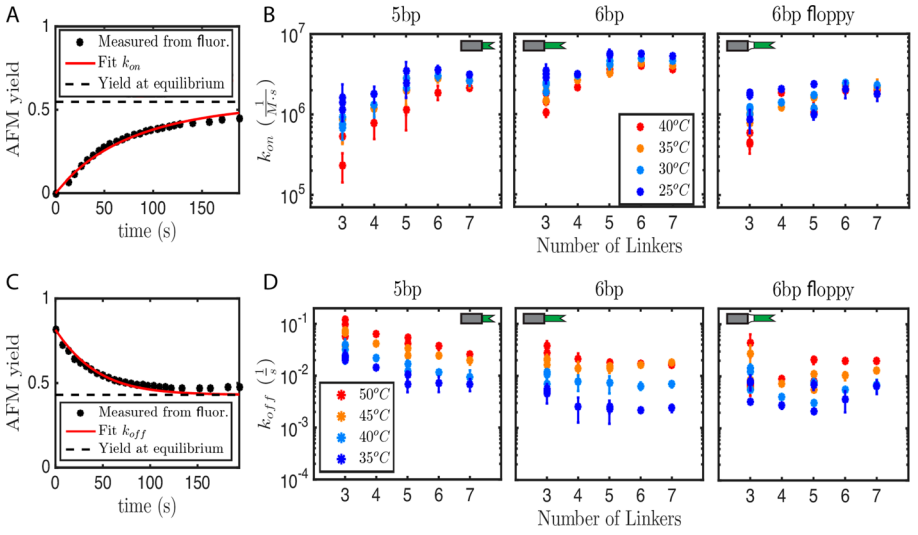

Figure 3. Reaction rate constants for multivalent DNA origami dimerization. (A) A temperature jump experiment used to measure k_{on} for one dimerization reaction (e.g., from 50 to 25 °C). For each such experiment, the k_{on} is determined by fitting the data to a second-order reaction with a known equilibrium constant. (B) k_{on} as a function of temperature, linker design, and the number of linkers for the (left) 5 bp SE linkers, (middle) 6 bp SE linkers, and (right) 6 bp floppy SE linkers. (C) A temperature jump experiment (e.g., from 25 to 50 °C) used to measure k_{off} for one dimerization reaction. (D) k_{off} as a function of temperature, linker design, and number of linkers for the (left) 5 bp SE linkers, (middle) 6 bp SE linkers, and (right) 6 bp floppy SE linkers. Inset linker diagram depicts the type of linker. Error bars indicate one standard deviation of the reported quantity and in some cases are too small to see.

Two Linear van't Hoff Fits Most Accurately Describe Multivalent DNA Origami Dimerization. Our next goal was to measure thermodynamic parameters, $\Delta H°$ and $\Delta S°$, of dimerization. For each dimerization reaction, we plotted the log of the equilibrium constant, $\ln(K_{eq})$, for binding as a function of inverse temperature to create a van't Hoff plot. For a simple chemical reaction, a van't Hoff plot should show a linear relationship between inverse temperature, with the slope corresponding to $-\Delta H°/R$ and the y-intercept corresponding to $\Delta S°/R$, which is what we observed for two of the 5 bp 3SE interfaces. However, for all other interfaces, we observed a nonlinear relationship between $\ln(K_{eq})$ and inverse temperature. Specifically, we observed that two linear fits to the van't Hoff plot, one at high temperatures (~40−55 °C, labeled "van't Hoff fit 1") and another at low temperatures (~25−40 °C, labeled "van't Hoff fit 2"), were appropriate (Supporting Information, Figures S7−S12). At high temperatures, K_{eq} changed rapidly, likely a result of interactions occurring between well-formed interfaces (i.e., interfaces with defect-free linkers bound to defect-free components). At lower temperatures, K_{eq} changed less dramatically, possibly because (1) some interfaces are defective (i.e., they contain less than their specified number of full-length linkers) due to truncation errors in DNA synthesis, (2) origami tiles are malformed, creating variable energetics between components, and/or (3) for 6 bp linkers the free linkers compete with origami to bind to an an interface, thus slowing or disallowing origami dimerization. This dimerization model also explains the broad (typically >20 °C) melting transition we observed: we are not simply observing one reaction happening between well-formed components with well-formed interfaces, but instead, are observing multiple reactions occurring between a distribution of components and their interfaces, thus leading to a broad melting transition. Therefore, when we examine the $\Delta H°$, $\Delta S°$, and $\Delta G°$ for each interface, we believe the van't Hoff at higher temperatures is likely to reflect more accurately the interaction energy of the well-formed interface (Supporting Information, Tables S1−S3 and Figures S15 and S16).

Next, we wanted to characterize the kinetics of origami dimerization as a function of interface design and solution temperature. To measure the forward (k_{on}) and reverse (k_{off}) reaction rates, we performed temperature jump experiments, a technique that has been widely used for studying interaction kinetics of biomolecular complexes, especially between complementary RNA or DNA strands,[30,31] and monitored reaction progress with a fluorescence quenching assay. In these experiments, we perturbed the system from equilibrium by either rapidly cooling the solution from a higher temperature to a final lower temperature (to determine k_{on}) or heating the solution from a lower temperature to a final higher temperature (to determine k_{off}) (see the methods and Supporting Information, Note 4). From fluorescence measurements, we obtained the dimer yield as a function of time and performed a least-squares fit of k_{on} to the eq (Figure 3A)

$$\frac{\mathrm{d(yield)}}{\mathrm{d}t} = k_{on}\left((1 - \mathrm{yield})^2 C_0 - \frac{\mathrm{yield}}{K_{eq}}\right) \quad (1)$$

where C_0 is the initial concentration of an origami component and K_{eq} is the equilibrium constant, defined mathematically as $K_{eq} = \frac{[D]_{eq}}{[T1]_{eq}[T2]_{eq}} = \frac{\mathrm{yield}_{eq}}{C_0(1-\mathrm{yield}_{eq})^2}$ where $[D]_{eq}$, $[T1]_{eq}$, and $[T2]_{eq}$ are the concentrations of dimer, T1, and T2, respectively, at equilibrium and yield_{eq} is the yield at equilibrium. Values of yield_{eq} for all temperatures studied were experimentally determined from the anneal/melt experiments. Similarly, to determine the first-order reverse rate constant, we fit k_{off} to the following eq (Figure 3C):

$$\frac{\mathrm{d(yield)}}{\mathrm{d}t} = k_{off}[K_{eq}(1 - \mathrm{yield})^2 C_0 - \mathrm{yield}] \quad (2)$$

Interestingly, we found that forward reaction rates for all interface designs are in the range of ~10^5−10^6 $(\mathrm{M \cdot s})^{-1}$ (Figure

DOI: 10.1021/jacs.5b10502
J. Am. Chem. Soc. 2016, 138, 3346−3354

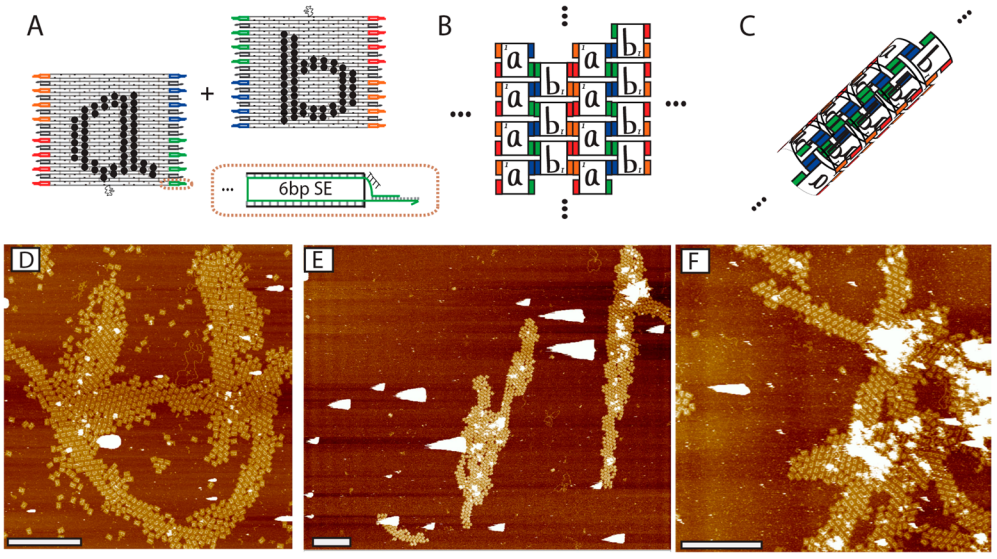

Figure 4. Two-dimensional origami tile lattice with two tiles labeled "a" and "b" designed with four 6 bp SEs per interface. (A) Schematic of tiles a and b that form a lattice. These tiles are structurally identical to T1 and T2, except for the hairpin staples and linking schematic. For simplicity, linker edges are shown in a uniform color, although each SE sequence and scaffold−linker complementary region have unique sequences and are not self-complementary. Schematic of (B) 2D lattice (intended) and (C) tube (unintended) as possible confirmations of the a−b lattice. AFM images of origami lattices annealed with different protocols: (D) from 55 to 44 °C at a rate of −0.5 °C/h, (E) from 55 to 36 °C at a rate of −0.5 °C/h, and (F) from 55 to 38 °C at a rate of −1 °C/h. Scale bars located at the bottom left of the AFM images are 1 μm.

3B and Supporting Information, Figures S17−S22), similar in scale to bimolecular association rates for both smaller double-cross-over DNA tiles, which range from ∼10^5 to 10^6 $(M{\cdot}s)^{-1}$,[14c,d] and DNA oligonucleotides, which range from ∼10^6 to $10^7(M{\cdot}s)^{-1}$.[32] Furthermore, at the temperatures we tested (45−25 °C), the forward reaction rate constants do not monotonically increase with increasing temperature, as would be expected for many bimolecular chemical reactions[33] or even dimerization of DNA nanostructures at lower temperatures.[14c] Such non-Arrhenius behavior has been previously reported in multiple studies of dsDNA duplex formation[34] and is explained by the prevailing model of successful DNA duplex formation.[34a,35] In this model, dimerization begins via a slow nucleation step involving two or three bases on either helix aligning to nucleate a metastable intermediate and then proceeds through a fast zipping-up mechanism to form the complex. In short, non-Arrhenius behavior arises from the fact that more bases are required to form a nucleus at higher temperatures, making the nucleation rate and thus the overall forward reaction rate slower.[35] Thus, we did not observe clear trends for k_{on} with temperature, as we would expect to see if we explored lower temperatures (∼10−25 °C), where the number of bases needed to nucleate the formation of a duplex is constant.[35] The maximum value for k_{on} was found to be 5.7×10^6 $(M{\cdot}s)^{-1}$ for multiple 6 bp interfaces at 25 °C, a similar order of magnitude for complementary DNA oligonucleotides for components with multiple architectures of 6 bp interfaces (Supporting Information, Figures S19 and S20). At the same temperature, the minimum value of k_{on} for interfaces that produced larger than a 50% yield was the floppy three SE interface with a value of 8.6×10^5 $(M{\cdot}s)^{-1}$, which is more than 5 times slower than the fastest reaction rate constant. Such a degree of difference in rates suggests that one could use this information to tune the rate of assembly as a method for controlling the assembly pathways.

Increasing the Number of Linkers Per Interface Tends To Increase Rates of Association. Additionally, multiple short SEs led to faster association rates than fewer SEs. This finding is consistent with findings in small DNA tile dimerization.[14c] Multivalent interactions increase the dimerization probability because they increase the frequency of nucleation: as the first SE partially hybridizes to its complementary SE, the effective concentration of complementary SEs increases. Intuitively, this makes sense because a greater number of linkers provides more opportunities for the SEs to nucleate an intermediate before zipping up. Floppy linkers have lower association rate constants than their nonfloppy counterparts, possibly due to the fact that upon nucleation with one or more complementary SEs, the other floppy linkers' SEs are likely misaligned, requiring more nucleation events to occur on average before a successful dimerization event.

Increasing the Number of Nonfloppy Linkers Per Interface Tends To Decrease Rates of Dissociation. As we expect for all interfaces, we found that k_{off} increased or stayed approximately the same with increasing temperature (Figure 3D and Supporting Information, Figures S23−S28). In general, shorter SEs produce higher k_{off} values at a given temperature and number of linkers. Values of k_{off} for interfaces with 5 bp SEs tended to decrease logarithmically with the number of linkers at a given temperature. Interestingly, 6 bp linkers generally had constant k_{off} values at a given temperature for interfaces with more than three linkers, while floppy linkers had no clear trend for k_{off} with the number of linkers. We compared the methods for generating K_{eq}, either by fitting k_{on} and k_{off} or by measuring the component concentrations at equilibrium, and found in most cases the separate, although not independent, measurements produced similar values (Supporting Information, Figure S29).

Extending the Two-Component Origami Dimer System to a 2D "Infinite" Lattice Enables Growth of Large Structures, Including Tubes. Finally, we sought to use our findings of the thermodynamics and kinetics measurements of interfaces to optimize the assembly of a two-

DOI: 10.1021/jacs.5b10502
J. Am. Chem. Soc. 2016, 138, 3346−3354

component, infinite lattice with multiple interfaces. As the interface with 6 bp SE and four linkers produced high yields and a favorable T_m (i.e., above the temperature at which nonspecific aggregation and linker interference become prevalent and below the origami component melting temperature), we designed two origami tiles with four different sets of interfaces with four linkers and 6 bp SEs that upon successful assembly would produce a diagonal two-dimensional cocrystal with a repeating pattern similar to a perpendicular striped design.[36] We labeled the tiles with hairpins "a" and "b" (Figure 4A) to distinguish them. Our strategy for 2D lattice assembly was to anneal in highly reversible regimes (i.e., where the derivative of the melt/anneal curve is a maximum and just below, specifically, 40−50 °C) with slow cooling, to promote growth of large, defect-free lattices.[37] In designing this annealing process, we assumed that all of the interfaces have identical kinetic and thermodynamic constants and thus expect the extent of growth and growth rates for all interface directions to be equal, but that might not be the case.[23]

We expected that flat origami components would grow to produce a flat 2D lattice (Figure 4B) and found that indeed lattices grew and produced large structures, up to 8 μm^2, with relatively few defects (Figure 4D,F and Supporting Information, Figure S31). We also found that along with flat lattices, tubes form in solution (Figure 4C) and then unfurl on the mica surface, as evidenced on the AFM by a constant width lattice, with lengths approaching 10 μm (Figure 4E and Supporting Information, Figure S31). After finding evidence for large, tubelike structures forming in solution with the 6 bp linkers, we hypothesized that the 6 bp floppy linkers might be more conducive to forming extended lattice structures, as the flexibility in the linker might increase the entropic penalty for forming a tube. However, we also observed lattices consistent with nanotube formation when using the floppy linker, including some large 2D flat lattices with defects and long, constant width lattices suggesting tubelike structures in solution (Supporting Information, Note 5). Furthermore, the floppy linkers produced lattices with a higher number of defects, as observed in the constant width structures on the AFM images, suggesting that nonfloppy linkers provide more structural stability for large lattices than floppy linkers.

Other attempts to cocrystallize a planar infinite lattice from two rectangular origami components, such as that by Liu et al.,[38] have produced structures with high aspect ratios, which are consistent with tube formation. Our findings here echo those observations and support the authors' subsequent strategy of designing components that allow helical axis-only growth by using components with orthogonal helical domains. Our findings reinforce this idea for rectangular, single-layer origami components: growth along the transverse axis (i.e., perpendicular to the helical axis) is likely to result in tubular structures.

CONCLUSION

Using fluorescence quenching assays and AFM calibration, we investigated how the structure of Watson−Crick base pair driven interfaces control the thermodynamics and kinetics of origami assembly. We found that equilibrium is rapidly achieved with interfaces composed of multiple short SE domains and that increasing the number of linkers per interface tended to increase the forward reaction rate and decrease the reverse reaction rate, suggesting that multiple linkers work together both to speed up the reaction and to stabilize the dimer. We found that the kinetic and thermodynamic properties (e.g.,T_m, k_{on}) of a self-assembly system can be tuned by manipulating the interface architecture (e.g., number of linkers, length of SEs). Furthermore, some "floppiness" in linker design decreases the thermal stability, yield, and reaction rates (i.e., lower k_{on}) as compared to nonfloppy linkers, likely as a result of the increased entropic penalty associated with aligning the SEs. When comparing infinite lattices with nonfloppy linkers to those with floppy linkers, we found the nonfloppy linkers produced structures with fewer defects. Therefore, generally speaking, introducing floppiness into a linker is an unfavorable design strategy.

The ability to design biomolecular interfaces with tailored kinetic and thermodynamic properties is essential to reliably control self-assembly. The kind of analysis used in this study (i.e., one that gives useful assembly parameters such as yield, k_{on}, and k_{off}) will be helpful to being able to build and control assembly processes, as well as engineer the assembly pathways.[39] At the moment, we cannot predict thermodynamic and kinetic properties of an interface given the number of linkers and the length of their SEs, for example, but it will be important to develop theories or models that accurately describe these aspects of DNA nanostructure assembly. The experimental methods developed here will be important for providing input for developing these models and for testing them. Ultimately, by tuning the strengths of interfaces as well as their kinetic properties, finite structures and infinite lattices can be built reliably.

This work suggests that while proper interface structure can improve the yields of origami assembly, other effects, such as the fidelity of the interface and the structure of the origami components themselves, are likely to be important in achieving reliable hierarchical assembly of origami structures. As evidenced by the tube formation in assembling "infinite" lattices, component curvature and flexibility play an important role in determining the final self-assembled structure.

MATERIALS AND METHODS

Self-Assembly of DNA Nanostructures. We obtained the m13mp18 ssDNA scaffold from Bayou Biolabs and all ssDNA staples from Integrated DNA Technologies (IDT) in RNase-free water at a stock concentration of 100 μM. All DNA strands were purchased with standard desalting, except for the fluorophore and quencher strands, which were HPLC-purified, and PAGE-purified linkers were ordered. Unless otherwise noted, all experiments were performed at the following concentrations: 10× body staples, 5× blocker staples, and 3× linker staples, where "×" indicates the concentration relative to the scaffold. The scaffold concentration was 10 nM. All samples were prepared in TAE/12.5 mM magnesium acetate tetrahydrate (TAE Mg^{2+}) buffer at a volume of 150 μL.

AFM Yield Measurements. AFM samples were handled under isothermal conditions, using a glovebox with PID fan temperature control (Coy Laboratories). Buffers, pipettes, pipet tips, Scotch tape, and mica puck were left in the glovebox for at least 30 min prior to sample prep in order to achieve thermal equilibrium. We then deposited 3 μL of sample on the mica surface and performed three buffer washes with TAE Mg^{2+} in order to eliminate loosely adsorbed staple strands. To hinder origami dimerization on the mica surface, we then applied TAE Mg^{2+} also containing 5 mM nickel(II) acetate tetrahydrate in order to strongly adsorb the DNA nanostructures to the mica surface.[40] The sample was imaged at room temperature.

Kinetics and Thermodynamics Measurements. All fluorescence readings were performed using either a MX3005P or MX3000P Stratagene qPCR. The two origami tiles to undergo dimerization were mixed and placed in the real-time thermal cycler at room temperature.

DOI: 10.1021/jacs.5b10502
J. Am. Chem. Soc. 2016, 138, 3346−3354

Thermodynamic data were obtained by repeatedly (at least twice, see Supporting Information, Notes 2 and 3) melting the solution by heating it to 55 °C and then annealing it to 25 °C at a rate of ±1 °C/15 min, unless otherwise noted. To ensure that measurements were repeatable and to eliminate any initial noise associated with the fluorophore strand, which occurred on the first heating or cooling cycle (Supporting Information, Note 2), measurements were collected over two heating and cooling cycles. Kinetics measurements were performed immediately after thermodynamic measurements and were obtained by rapidly heating (at a rate of 2.5 °C/s) the sample from 25 °C to a given temperature (in the case of measuring forward reaction rates) or by rapidly cooling (at a rate of −2.5 °C/s) from 55 °C (in the case of measuring reverse reaction rates) and monitoring the fluorescence in intervals of 2−6 s. All fluorescence measurements were performed at least in triplicate.

2D Infinite Lattice Formation. All samples were plated and imaged using the same temperature-controlled protocol as the AFM dimer yield measurements.

■ ASSOCIATED CONTENT

Supporting Information

. The Supporting Information is available free of charge on the ACS Publications website at DOI: 10.1021/jacs.5b10502.

Includes further data and analysis and an explanation of thermodynamic and kinetic measurements (PDF)
DNA sequences used (XLSX)

■ AUTHOR INFORMATION

Corresponding Author

*rschulm3@jhu.edu

Notes

The authors declare no competing financial interest.

■ ACKNOWLEDGMENTS

This work was supported by NSF awards CCF-1161941 and CMMI-1253876 (CAREER) to RS, a Turing Scholar Award from the John Templeton foundation and Johns Hopkins University startup funds. We also acknowledge DOE BMES grant DE-SC0010595 for materials, supplies and computational tools. The authors would like to thank Abdul Mohammed, Joshua Fern, Dominic Scalise, Deepak Agarwal, and Angelo Cangalosi for helpful discussions regarding this work and Jennifer Lu for designing the "A" and "B" hairpins for the infinite lattice.

■ ABBREVIATIONS USED

T1, tile 1; T2, tile 2; D, dimer; SE, sticky end; bp, base pair; AFM, atomic force microscopy; VH, van't Hoff; Thy4, polythymine (four consecutive thymine bases)

■ REFERENCES

(1) Rothemund, P. W. K. *Nature* **2006**, *440* (7082), 297−302.

(2) Pinheiro, A. V.; Han, D. R.; Shih, W. M.; Yan, H. *Nat. Nanotechnol.* **2011**, *6* (12), 763−772.

(3) (a) Fu, J. L.; Liu, M. H.; Liu, Y.; Woodbury, N. W.; Yan, H. *J. Am. Chem. Soc.* **2012**, *134* (12), 5516−5519. (b) Linko, V.; Eerikainen, M.; Kostiainen, M. A. *Chem. Commun.* **2015**, *51* (25), 5351−5354. (c) Voigt, N. V.; Torring, T.; Rotaru, A.; Jacobsen, M. F.; Ravnsbaek, J. B.; Subramani, R.; Mamdouh, W.; Kjems, J.; Mokhir, A.; Besenbacher, F.; Gothelf, K. V. *Nat. Nanotechnol.* **2010**, *5* (3), 200−203.

(4) (a) Andersen, E. S.; Dong, M.; Nielsen, M. M.; Jahn, K.; Subramani, R.; Mamdouh, W.; Golas, M. M.; Sander, B.; Stark, H.; Oliveira, C. L. P.; Pedersen, J. S.; Birkedal, V.; Besenbacher, F.; Gothelf, K. V.; Kjems, J. *Nature* **2009**, *459* (7243), 73−U75. (b) Zadegan, R. M.; Jepsen, M. D. E.; Hildebrandt, L. L.; Birkedal, V.; Kjems, J. *Small* **2015**, *11* (15), 1811−1817. (c) Zadegan, R. M.; Jepsen, M. D. E.; Thomsen, K. E.; Okholm, A. H.; Schaffert, D. H.; Andersen, E. S.; Birkedal, V.; Kjems, J. *ACS Nano* **2012**, *6* (11), 10050−10053.

(5) (a) Gu, H. Z.; Chao, J.; Xiao, S. J.; Seeman, N. C. *Nature* **2010**, *465* (7295), 202−U86. (b) Lund, K.; Manzo, A. J.; Dabby, N.; Michelotti, N.; Johnson-Buck, A.; Nangreave, J.; Taylor, S.; Pei, R. J.; Stojanovic, M. N.; Walter, N. G.; Winfree, E.; Yan, H. *Nature* **2010**, *465* (7295), 206−210.

(6) (a) Marras, A. E.; Zhou, L. F.; Su, H. J.; Castro, C. E. *Proc. Natl. Acad. Sci. U. S. A.* **2015**, *112* (3), 713−718. (b) Gerling, T.; Wagenbauer, K. F.; Neuner, A. M.; Dietz, H. *Science* **2015**, *347* (6229), 1446−1452. (c) Zhou, L. F.; Marras, A. E.; Su, H. J.; Castro, C. E. *ACS Nano* **2014**, *8* (1), 27−34.

(7) (a) Schulman, R.; Winfree, E. *Siam J. Comput* **2010**, *39* (4), 1581−1616. (b) Mohammed, A. M.; Schulman, R. *Nano Lett.* **2013**, *13* (9), 4006−13.

(8) (a) Douglas, S. M.; Bachelet, I.; Church, G. M. *Science* **2012**, *335* (6070), 831−834. (b) Zhang, Q.; Jiang, Q.; Li, N.; Dai, L. R.; Liu, Q.; Song, L. L.; Wang, J. Y.; Li, Y. Q.; Tian, J.; Ding, B. Q.; Du, Y. *ACS Nano* **2014**, *8* (7), 6633−6643.

(9) (a) Hariadi, R. F.; Cale, M.; Sivaramakrishnan, S. *Proc. Natl. Acad. Sci. U. S. A.* **2014**, *111* (11), 4091−4096. (b) Langecker, M.; Arnaut, V.; Martin, T. G.; List, J.; Renner, S.; Mayer, M.; Dietz, H.; Simmel, F. C. *Science* **2012**, *338* (6109), 932−936.

(10) Marchi, A. N.; Saaem, I.; Vogen, B. N.; Brown, S.; LaBean, T. H. *Nano Lett.* **2014**, *14* (10), 5740−7.

(11) Zhao, Z.; Liu, Y.; Yan, H. *Nano Lett.* **2011**, *11* (7), 2997−3002.

(12) Rajendran, A.; Endo, M.; Katsuda, Y.; Hidaka, K.; Sugiyama, H. *ACS Nano* **2011**, *5* (1), 665−671.

(13) Woo, S.; Rothemund, P. W. K. *Nat. Commun.* **2014**, *5*, 4889.

(14) (a) Wei, X. X.; Nangreave, J.; Liu, Y. *Acc. Chem. Res.* **2014**, *47* (6), 1861−1870. (b) Nangreave, J.; Yan, H.; Liu, Y. *Biophys. J.* **2009**, *97* (2), 563−571. (c) Jiang, S. X.; Yan, H.; Liu, Y. *ACS Nano* **2014**, *8* (6), 5826−5832. (d) Hariadi, R. F.; Yurke, B.; Winfree, E. *Chem. Sci.* **2015**, *6* (4), 2252−2267.

(15) (a) Sobczak, J. P. J.; Martin, T. G.; Gerling, T.; Dietz, H. *Science* **2012**, *338* (6113), 1458−1461. (b) Han, D. R.; Pal, S.; Yang, Y.; Jiang, S. X.; Nangreave, J.; Liu, Y.; Yan, H. *Science* **2013**, *339* (6126), 1412−1415. (c) Douglas, S. M.; Marblestone, A. H.; Teerapittayanon, S.; Vazquez, A.; Church, G. M.; Shih, W. M. *Nucleic Acids Res.* **2009**, *37* (15), 5001−5006. (d) Bai, X. C.; Martin, T. G.; Scheres, S. H. W.; Dietz, H. *Proc. Natl. Acad. Sci. U. S. A.* **2012**, *109* (49), 20012−20017.

(16) Gonen, S.; DiMaio, F.; Gonen, T.; Baker, D. *Science* **2015**, *348* (6241), 1365−1368.

(17) King, N. P.; Sheffler, W.; Sawaya, M. R.; Vollmar, B. S.; Sumida, J. P.; Andre, I.; Gonen, T.; Yeates, T. O.; Baker, D. *Science* **2012**, *336* (6085), 1171−1174.

(18) Rohl, C. A.; Strauss, C. E. M.; Misura, K. M. S.; Baker, D. *Methods Enzymol.* **2004**, *383*, 66−93.

(19) Seeman, N. C. *Nature* **2003**, *421* (6921), 427−431.

(20) Woo, S.; Rothemund, P. W. K. *Nat. Chem.* **2011**, *3* (8), 620−627.

(21) (a) Kim, D. N.; Kilchherr, F.; Dietz, H.; Bathe, M. *Nucleic Acids Res.* **2012**, *40* (7), 2862−8. (b) Castro, C. E.; Kilchherr, F.; Kim, D. N.; Shiao, E. L.; Wauer, T.; Wortmann, P.; Bathe, M.; Dietz, H. *Nat. Methods* **2011**, *8* (3), 221−229.

(22) Li, Z.; Wang, L.; Yan, H.; Liu, Y. *Langmuir* **2012**, *28* (4), 1959−1965.

(23) Fern, J.; Lu, J.; Schulman, R. *ACS Nano* **2016**, *10*, 1836.

(24) Wang, R. S.; Kuzuya, A.; Liu, W. Y.; Seeman, N. C. *Chem. Commun.* **2010**, *46* (27), 4905−4907.

(25) Wang, J. C. *Proc. Natl. Acad. Sci. U. S. A.* **1979**, *76* (1), 200−203.

(26) (a) SantaLucia, J. *Proc. Natl. Acad. Sci. U. S. A.* **1998**, *95* (4), 1460−1465. (b) Schulman, R.; Winfree, E. *Proc. Natl. Acad. Sci. U. S. A.* **2007**, *104* (39), 15236−15241. (c) Rothemund, P. W. K.; Papadakis, N.; Winfree, E. *PLoS Biol.* **2004**, *2* (12), 2041−2053.

(27) You, Y.; Tataurov, A. V.; Owczarzy, R. *Biopolymers* **2011**, *95* (7), 472−486.

DOI: 10.1021/jacs.5b10502
J. Am. Chem. Soc. 2016, 138, 3346−3354

(28) Rice, S. A.; Doty, P. *J. Am. Chem. Soc.* **1957**, *79* (15), 3937–3947.
(29) Dreyfus, R.; Leunissen, M. E.; Sha, R. J.; Tkachenko, A. V.; Seeman, N. C.; Pine, D. J.; Chaikin, P. M. *Phys. Rev. Lett.* **2009**, *102* (4), 048301.
(30) Williams, A. P.; Longfellow, C. E.; Freier, S. M.; Kierzek, R.; Turner, D. H. *Biochemistry* **1989**, *28* (10), 4283–4291.
(31) (a) Porschke, D.; Uhlenbeck, O. C.; Martin, F. H. *Biopolymers* **1973**, *12* (6), 1313–1335. (b) Nelson, J. W.; Tinoco, I. *Biochemistry* **1982**, *21* (21), 5289–5295.
(32) (a) Gao, Y.; Wolf, L. K.; Georgiadis, R. M. *Nucleic Acids Res.* **2006**, *34* (11), 3370–3377. (b) Morrison, L. E.; Stols, L. M. *Biochemistry* **1993**, *32* (12), 3095–104. (c) Zhang, D. Y.; Winfree, E. *J. Am. Chem. Soc.* **2009**, *131* (47), 17303–14.
(33) Logan, S. R. *J. Chem. Educ.* **1982**, *59* (4), 279–281.
(34) (a) Craig, M. E.; Crothers, D. M.; Doty, P. *J. Mol. Biol.* **1971**, *62* (2), 383. (b) Chen, C. L.; Wang, W. J.; Wang, Z.; Wei, F.; Zhao, X. S. *Nucleic Acids Res.* **2007**, *35* (9), 2875–2884.
(35) Ouldridge, T. E.; Sulc, P.; Romano, F.; Doye, J. P. K.; Louis, A. A. *Nucleic Acids Res.* **2013**, *41* (19), 8886–8895.
(36) Rothemund, P. W. K.; Ekani-Nkodo, A.; Papadakis, N.; Kumar, A.; Fygenson, D. K.; Winfree, E. *J. Am. Chem. Soc.* **2004**, *126* (50), 16344–16352.
(37) Zenk, J.; Schulman, R. *PLoS One* **2014**, *9* (10), e111233.
(38) Liu, W. Y.; Zhong, H.; Wang, R. S.; Seeman, N. C. *Angew. Chem., Int. Ed.* **2011**, *50* (1), 264–267.
(39) (a) Deeds, E. J.; Bachman, J. A.; Fontana, W. *Proc. Natl. Acad. Sci. U. S. A.* **2012**, *109* (7), 2348–2353. (b) Levy, E. D.; Erba, E. B.; Robinson, C. V.; Teichmann, S. A. *Nature* **2008**, *453* (7199), 1262–U66.
(40) Hansma, H. G.; Laney, D. E. *Biophys. J.* **1996**, *70* (4), 1933–1939.

DOI: 10.1021/jacs.5b10502
J. Am. Chem. Soc. 2016, 138, 3346–3354